Computer Assisted Mechanics and Engineering Sciences, 7: 343–362, 2000.

FEM analysis of binary dilute system solidification using the anisotropic porous medium model of a mushy zone

Jerzy Banaszek and Piotr Furmański
Institute of Heat Engineering, Warsaw University of Technology, Nowowiejska 25, 00-665 Warsaw, Poland

(Received October 14, 1999)

Finite Element Method (FEM) calculations have been performed to address the problem of the influence of anisotropy of permeability and of thermal conductivity of a mushy region on a temporary flow pattern and temperature during solidification of binary mixtures. Computationally effective FEM algorithm is based on the combination of the projection method, the semi-implicit time marching scheme and the enthalpy–porosity model of the two-phase region. Example calculations are given for two different dilute solutions of ammonium chloride and water. The effect of permeability anisotropy considerably changes the shape of the mushy zone. Three different models of thermal conductivity, the first – based on a mixture theory, the second – fully anisotropic one and the third – the model of isotropic effective conductivity, have been analyzed and mutually compared. It has been found that the impact of the thermal conductivity anisotropy is visible only in the case when this property differs significantly in both phases.

1. Introduction

Solidification of a binary system occurs over a range of temperatures and a two-phase solid–liquid region of a finite volume, called the mushy zone, separates the fully liquid and fully solid domains. Solid within the multiphase region appears in the form of a dense crystalline-like matrix. The extremely complex nature of this solid formation exhibits preferred growth mechanisms and selective directionality that are function of local temperatures and compositions. Moreover, since the liberation of latent heat occurs at the microscopic interfaces that separate the phases, energy evolution within the mushy region depends on complex morphology of these interfaces. Compounding these difficulties is the fact that liquid flow, in both the bulk liquid region (forced convection, buoyancy forces) and in the mushy zone (flow of the liquid phase through the dendritic array) significantly influences the solidification process. The thermodynamic and transport properties vary continuously over the whole domain of the mushy zone. Moreover, the strongly directional nature of the dendrites results in anisotropy of flow resistance through the dendritic array and in anisotropy of thermal properties.

Despite this complex nature of binary solid–liquid phase change and difficulties arising from strong and nonlinear couplings between the velocity, pressure, temperature and concentration fields, significant advances have been made in mathematical modeling and computer simulation of the solid–liquid phase transition of binary systems. This progress has been stimulated by the engineering importance of the quantitative analysis of all transport processes of the solid–liquid phase transition in binary systems, for example, in material processing and latent heat energy storage systems. Moreover, difficulty in experimental discerning of convection pattern in molten metals renders numerical simulation especially attractive. Bennon and Incropera [3] have developed a continuum model for the prediction of macroscopic transport behavior of binary phase change systems where the two-phase region can be viewed as a fluid saturated porous medium. The continuum equations of this model, that govern the conservation of mass, momentum, energy and species, are given in

terms of mixture quantities and they remain valid in all regions (solid, liquid and mushy) of the phase change domain [3]. They are very similar to standard single-flow equations, and thus, easier for numerical simulation and solution than the complete two-phase flow set of equations. Moreover, this approach allows avoiding direct modeling of the interface exchange conditions that in many practical problems have not yet been well established. Therefore, the continuum model has been widely used in both finite difference [4, 17, 23, 26] and FEM discretization techniques [7, 19], and it is also applied in the present study.

The strongly directional nature of dendrite growth results in anisotropy of flow conditions and thermophysical properties in the mushy zone. For high volumetric liquid fraction, flow along the primary dendrite direction is accompanied by a cross-flow normal to this direction. This can produce higher (than in the Blake–Kozeny flow model [3]) pressure drops, and thus it can cause significant change in the flow resistance of the porous medium. Poirier [16] has shown that the permeability, the intrinsic property that characterizes this resistance, is vastly different in direction parallel and normal to the dendrites. One can also expect that directional dendritic morphology can affect heat conduction process in the mushy zone, i.e. the anisotropy of thermal conductivity and thermal diffusivity can appear. Therefore, in order to retain physics of the analyzed phenomena in their numerical modeling, the anisotropy of flow conditions and thermal properties in the mushy zone should be accounted for.

Unfortunately, these important aspects have largely been ignored. Indeed, there are only a few papers that address the problem of a directional character of permeability of the two-phase region [15, 16, 19]. Moreover, to the authors' knowledge, the impact of thermal conductivity anisotropy and of thermal dispersion on heat transfer in the mushy zone has not yet been reported in the literature. Dispersion essentially results from two mechanisms [1, 9], i.e. mixing of the local fluid streams as fluid follows via tortuous paths around solid dendrites and enhancement of the mutual solid–fluid thermal interaction due to increase of the local temperature gradient caused by the fluid flow. In mathematical modeling dispersion can be accounted for by additional diffusive term in the energy equation, which is dependent of the local fluid velocity.

Therefore, to get a better understanding of complex fluid flow and heat transfer phenomena in a solidifying binary system, our study is focused on a numerical analysis of the influence of all above discussed effects on velocity and temperature fields and on a temporary shape of the mushy zone in a solidifying dilute binary mixture.

The computational model developed is based on the finite element spatial discretization and on some solving techniques that accelerate calculations. The cost effectiveness of FEM continues to be significant in the computer simulation of joint fluid flow and heat transfer problems. The problem is even more crucial in modeling of phase change phenomena in binary systems, where strong couplings occur between pressure, velocity, temperature and concentration fields. It is commonly known that the finite difference method is superior in terms of computer storage and CPU time requirements when compared with the FEM analysis. This results from a less sparse form of FEM matrices, caused by the use of irregular grids and high-order polynomial interpolations of the unknown field property. But it also comes from the application of the simultaneous solution algorithms, where a whole set of continuity, Navier–Stokes and energy equations is solved concurrently, as commonly used in the early FEM analysis of incompressible fluid flows [21, 22]. Therefore, over the last decade attempts have been made to improve the computational efficiency of FEM simulation of field theory problems through the use of various sophisticated acceleration techniques. Most of these techniques take their origin from the finite difference methods. Specifically,

- Approximate solution to the Navier–Stokes equations for an incompressible fluid can be found by the use of the projection method [6, 11], where velocity is uncoupled from pressure. The key word here is sequential which means first velocity is solved and then pressure, rather than simultaneously solving the coupled set of equations.
- Semi-implicit time marching scheme can be applied where viscous/diffusion terms are treated implicitly, whereas advection ones treated explicitly [11, 18]. The main attribute of this approach

is that it allows replacement of a set of the coupled fluid flow and heat transfer equations by several smaller symmetric linear systems solved sequentially through the use of effective algebraic solvers.

- In numerical modeling of solid–liquid phase change transition, the energy conservation can be analyzed via an enthalpy approach on a fixed grid [5, 20, 24, 25]. With a correctly defined enthalpy–temperature relation, the full effect of the latent heat can be accurately modeled without the need to know an exact position of the phase interface. And thus, a cumbersome front tracking algorithm is avoided.

The developed FEM numerical model and its computational algorithm are based on the combination of all aforementioned techniques (see the next section of the paper and [2] for more details). Prior to the use of this calculation tool in addressing questions of some physical and quantitative aspects of the phenomena considered, the credibility of its numerical predictions must be proved. It consists of two processes: code verification and validation. The verification procedure is based on grid refinement studies and comparisons with other available solutions of some benchmark problems. Although such a study is obviously necessary, it by itself is not sufficient to establish confidence in the numerically obtained predictions. Indeed, for engineers and scientists nature is the final jury. It means that the degree to which inevitable simplifications of physical and mathematical models reflect reality should be established. This code validation process is carried out by extensively comparing numerical results with trustworthy detailed experimental measurements. Both this procedures have been conducted for the developed numerical model and their details are given elsewhere [2]. The results, there reported, show satisfactory accuracy of the model for typical benchmark problems and its validity in the case of pure water solidification driven by conduction and buoyancy forces in a differentially heated square cavity.

On that basis, it is further assumed that the proposed numerical tool can provide reasonable predictions in the case of solidification of a dilute binary system. Hence, it is further used to address the problem of how the anisotropic morphology of the mushy zone influences a flow pattern and temperature field in two different dilute solutions of water and ammonium chloride filling a square cavity.

2. Mathematical model

On the onset of the analysis, let us make some assumptions that significantly simplify the mathematical model. They, however, still maintain the model capability for addressing the main objective of the study – the question of the influence of anisotropic morphology in the mushy zone on velocity and temperature fields in a solidifying dilute solution. They are as follows.

1. Flow is laminar in two-dimensional geometry and the fluid is Newtonian and incompressible
2. Boussinesq approximation of constant liquid density and of linear dependence of buoyancy forces and temperature is valid, i.e.

$$g_i(\rho - \rho_{\mathrm{ref}}) = g_i \beta_T \left(T_{\mathrm{ref}} - T\right), \tag{1}$$

where g_i, β_T and ρ_{ref} are, respectively, i-component of the gravity acceleration vector, the thermal expansion coefficient and density at a reference temperature T_{ref}.

3. Solute mass transfer and buoyancy forces arising from concentration gradients are neglected. These phenomena can, in general, significantly affect flow and heat transfer processes. There are, however, not so crucial for dilute systems, where the solute concentration is very small. They are also not so important for the purpose of this study which is restricted to some comparative analysis performed in order to address the question of whether anisotropy of the dendritic region can be, or cannot be, ignored.

4. Only dilute solutions are analyzed where properties and enthalpy are only functions of temperature in the mushy zone.
5. The dendritic region is treated as a porous medium where the theory of mixtures is applied.
6. The solid phase is non-deforming and free of internal stresses, cavity boundaries are impermeable – these requirements cause assumption that densities of both phases are equal i.e. $\rho_L = \rho_S$. This implies the equivalence of mass and volume fractions of the mixture in the mushy zone.
7. The solid phase is stationary, i.e. components of the solid phase velocity $v_{iS} = 0$.

With these assumptions, mixture continuum equations for the conservation of mass, momentum and energy, which are obtained by adding pertinent equations for each phase [3], take the form

$$\frac{\partial v_i}{\partial x_i} = 0\,,$$

$$\rho \frac{\partial v_i}{\partial t} + \rho v_j \frac{\partial v_i}{\partial x_j} = -\frac{\partial p}{\partial x_i} + \frac{\partial}{\partial x_j}\left(\mu_L \frac{\partial v_i}{\partial x_j}\right) + g_i \beta_T (T_{\text{ref}} - T) + S_{v_i}\,, \tag{2}$$

$$\frac{\partial(\rho H)}{\partial t} + v_j \frac{\partial(\rho H_L)}{\partial x_j} = \frac{\partial}{\partial x_i}\left(\lambda_{ij} \frac{\partial T}{\partial x_j}\right),$$

where p, v_i, μ_L and λ_{ij} are, respectively, the motion pressure [10], components of the velocity vector, dynamic viscosity of the liquid phase and components of the thermal conductivity tensor. Upon the seventh assumption above

$$v_i = (1 - f) v_{iS} + f v_{iL} = f v_{iL} \tag{3}$$

where f is the volumetric liquid fraction, that, with the sixth assumption, is equal to the mass fraction. Components of the mixture thermal conductivity tensor λ_{ij} and the mixture total enthalpy per cubic meter (ρH) are discussed further in the paper.

Additional source term appears in the momentum equation to mimic the Carman–Blake–Kozeny model of flow in the mushy zone [3, 19, 23, 25] treated as a porous medium. It has the form

$$S_{v_i} = \mu_L K_{ij}^{-1} v_j \tag{4}$$

where K_{ij} are components of the permeability tensor.

3. FEM EQUATIONS AND COMPUTATIONAL ALGORITHM

Semi-discrete counterpart of the set of partial differential equations, Eq. (2), is obtained through the use of the FEM spatial discretization procedure along with the Galerkin weighted residual method [27]. First, the piece-wise interpolations of velocity, temperature and pressure fields are assumed in terms of sums of shape functions N_k or P_l and nodal values of the pertinent unknowns at grid points that form the finite element spatial discretization [27]

$$\begin{aligned} v_i(\bar{x}, t) &= N_k(\bar{\zeta})\, v_{ik}(t)\,, \\ T(\bar{x}, t) &= N_k(\bar{\zeta})\, T_k(t), \qquad \text{for } k = 1, 2, \ldots, NP\,, \\ p(\bar{x}, t) &= P_l(\bar{\zeta})\, p_l(t), \qquad \text{for } l = 1, 2, \ldots, NP_p\,, \end{aligned} \tag{5}$$

where the functions N_k and P_l are Lagrange polynomials defined in the local coordinate system $\bar{\zeta}$, which is related with the global coordinates x_i through one-to-one correspondence [27]

$$x_i(\bar{\zeta}) = N_k(\bar{\zeta}) x_{ik} \qquad \text{for } k = 1, 2, \ldots, NP\,. \tag{6}$$

To avoid spurious pressure modes of the FEM solution, the so-called unequal order interpolation is used where shape functions P_l are polynomials of one order less than polynomials N_k [2, 11, 27].

Next, including these approximations into Eq. (2) and weighting thus obtained residuals, over the whole analyzed domain Ω and through the functions P_l for the continuity equation and the functions N_k for the others, a set of ordinary differential equations (still differential in time) is obtained for the semi-discrete FEM model. It has the following matrix form

$$\begin{aligned}
&\mathbf{D}\cdot\mathbf{v}=\mathbf{0},\\
&\mathbf{M}\cdot\frac{\mathrm{d}\mathbf{v}_i}{\mathrm{d}t}+(\mathbf{K}^c(\mathbf{v})+\mathbf{K}^d)\cdot\mathbf{v}_i=-\mathbf{G}\cdot\mathbf{p}+\mathbf{F}_i \qquad \text{for } i=1,2,3,\\
&\mathbf{C}\cdot\frac{\mathrm{d}\mathbf{H}}{\mathrm{d}t}+\mathbf{K}_h^c(\mathbf{v})\cdot\mathbf{H}+\mathbf{K}_T^d\cdot\mathbf{T}=\mathbf{F}_T,
\end{aligned} \tag{7}$$

where $\mathbf{D}$, $\mathbf{M}$, $\mathbf{K}^d$, $\mathbf{K}^c$ and $\mathbf{G}$ are, respectively, the divergence, mass, diffusion, advection and pressure gradient matrices, whereas $\mathbf{C}$, $\mathbf{K}_h^c$ and $\mathbf{K}_T^d$ denote, respectively, the heat capacity, convection and conduction matrices. $\mathbf{v}_i$, $\mathbf{p}$, $\mathbf{H}$ and $\mathbf{T}$ stand for vectors of nodal values of velocity components, pressure, specific total enthalpy and temperature, respectively. Right-hand side vectors $\mathbf{F}_i$ and $\mathbf{F}_T$ of momentum and energy equations result, respectively, from body forces (buoyancy forces) and from velocity and thermal boundary conditions. Since detailed formulas for the matrices and right-hand side vectors can be found elsewhere, they are not repeated here.

The second discretization step is integration of Eq. (7) in time by a use of one, from many possible, time marching finite difference schemes. It leads to a final set of algebraic equations for a fully discrete FEM model. This step is a crucial point in developing of computationally efficient FEM algorithm. In the present study this aim is attained through the combination of the semi-implicit time marching scheme [11, 18] and separated calculations of pressure and velocity fields by application of the projection method [11].

First, pressure, which is an inherently implicit variable in an incompressible fluid model, must be treated implicitly. So the continuity equation has to be dealt with as such. One would be happy to extend this treatment to all other terms of the momentum and energy equations. Unfortunately, this approach creates the need for simultaneous solution of the whole set of fully coupled equations. In practice, this is prohibitively expensive and time-consuming, particularly for multi-dimensional problems. Therefore, we rather use the semi-implicit approach, where the viscous/diffusion terms of Eq. (7) are treated implicitly, whereas the advection/convection ones explicitly. In the developed algorithm the backward Euler scheme and the two-step explicit Adams–Bashforth method are used to get

$$\begin{aligned}
&\mathbf{D}\cdot\mathbf{v}^{n+1}=\mathbf{0},\\
&\mathbf{M}\cdot\frac{\mathbf{v}_i^{n+1}-\mathbf{v}_i^n}{\Delta t}+\mathbf{K}^d\cdot\mathbf{v}_i^{n+1}=\mathbf{F}_i-\mathbf{G}\cdot\mathbf{p}^{n+1}-\left(\frac{3}{2}\mathbf{K}^c(\mathbf{v}^n)\cdot v^n-\frac{1}{2}\mathbf{K}^c(\mathbf{v}^{n-1})\cdot\mathbf{v}^{n-1}\right),\\
&\mathbf{C}\cdot\frac{\mathbf{H}^{n+1}-\mathbf{H}^n}{\Delta t}+\mathbf{K}_T^d\cdot\mathbf{T}^{n+1}=\mathbf{F}_T-\left(\frac{3}{2}\mathbf{K}_h^c(\mathbf{v}^n)\cdot\mathbf{H}^n-\frac{1}{2}\mathbf{K}_h^c(\mathbf{v}^{n-1})\cdot\mathbf{H}^{n-1}\right),
\end{aligned} \tag{8}$$

where Δt is a time step, whereas superscripts $n-1$, n, $n+1$ stand for the previous, current and new times, respectively.

Further reduction of CPU time can be obtained by setting up an algorithm, where velocity calculations are uncoupled from pressure ones. In the presented code, the Projection Method [11] is adopted where at each time step calculations are performed in following three-step cycle:

For a given initial kinematics pressure p^n/ρ and divergence-free velocity field v_i^n with $\dfrac{\partial v_i^n}{\partial x_i}=0$

1. Solve the momentum equation for the intermediate velocity $\tilde{v}_i^{n+1}$

$$\frac{\partial\tilde{v}_i^{n+1}}{\partial t}+v_j^n\frac{\partial\tilde{v}_i^{n+1}}{\partial x_j}=\frac{\partial}{\partial x_j}\left(\vartheta\frac{\partial\tilde{v}_i^{n+1}}{\partial x_j}\right)+S_i$$

where

$$S_i = -\frac{1}{\rho}\frac{\partial p^n}{\partial x_i} - \vartheta K_{ij}^{-1} v_j^n \quad \text{and} \quad \tilde{v}_i = v_{ib} \quad \text{on } \Gamma.$$

2. Project this velocity vector onto the subspace of divergence-free vector field. This leads to the Poisson equation for the projection Lagrange multiplier Ψ [11]

$$\frac{\partial}{\partial x_i}\left(\frac{\partial \Psi}{\partial x_i}\right) = \frac{\partial \tilde{v}_i}{\partial x_i} \qquad \text{with} \qquad \frac{\partial \Psi}{\partial n} = 0 \quad \text{on } \Gamma$$

and correct the intermediate velocity in accordance with

$$v_i^{n+1} = \tilde{v}_i^{n+1} - \frac{\partial \Psi}{\partial x_i}.$$

3. Finally, the kinematics pressure is updated

$$\left(\frac{p^{n+1}}{\rho}\right) = \left(\frac{p^n}{\rho}\right) + \frac{2}{\Delta t}\Psi.$$

Thus, the projection cycle is completed. The FEM counterpart of this algorithm has the following matrix form

$$\begin{aligned}
&1.\ \mathbf{M}\cdot\frac{\tilde{\mathbf{v}}_i^{n+1}-\mathbf{v}_i^n}{\Delta t} + \mathbf{K}^d\cdot\tilde{\mathbf{v}}_i^{n+1} = \mathbf{F}_i - \mathbf{G}\cdot\mathbf{p}^n - \left(\frac{3}{2}\mathbf{K}^c(\mathbf{v}^n)\cdot\mathbf{v}^n - \frac{1}{2}\mathbf{K}^c(\mathbf{v}^{n-1})\cdot\mathbf{v}^{n-1}\right),\\
&2.\ \left.\begin{aligned}&\mathbf{G}^T\mathbf{M}^{-1}\mathbf{G}\cdot\Psi = -\mathbf{G}^T\cdot\tilde{\mathbf{v}}_i^{n+1},\\ &\mathbf{v}^{n+1} = \tilde{\mathbf{v}}_i^{n+1} - \mathbf{M}^{-1}\mathbf{G}\cdot\Psi,\end{aligned}\right\}\\
&3.\ \frac{\mathbf{p}^{n+1}}{\rho} = \frac{\mathbf{p}^n}{\rho} + \frac{2}{\Delta t}\Psi.
\end{aligned} \tag{9}$$

The energy equation is nonlinear due to temperature dependence of both the total enthalpy and thermophysical properties in the mushy zone. Therefore, following Swaminathan and Voller [20], an iterative process is constructed at each time step where:

For a given enthalpy–temperature curve $H(T)$ and $\mathbf{T}^m$ with $(\mathbf{T}^0 \equiv \mathbf{T}^n)$

1. calculate matrices $\mathbf{K}_T^d(\mathbf{T}^m)$ and $\mathbf{C}(\mathbf{T}^m)$,

2. replace the unknown current iteration of each nodal value H_k of the total specific enthalpy by its Taylor series expansion

$$H_k^{m+1} = H_k^m + \left(\frac{dH_k}{dT}\right)_m (T_k^{m+1} - T_k^m) \qquad \text{with} \quad T_k^m = H^{-1}(H_k^m) \tag{10}$$

to get the linearized energy equation

$$\begin{aligned}
&\left(\mathbf{K}_T^d(\mathbf{T}^m) + \frac{1}{\Delta t}\mathbf{C}(\mathbf{T}^m)\cdot\left(\frac{\mathrm{d}\mathbf{H}}{\mathrm{d}\mathbf{T}}\right)_m\right)\cdot\mathbf{T}^{m+1}\\
&\quad = \frac{1}{\Delta t}\mathbf{C}(\mathbf{T}^m)\cdot\left(\mathbf{H}^n - \mathbf{H}^m + \left(\frac{\mathrm{d}\mathbf{H}}{\mathrm{d}\mathbf{T}}\right)_m\cdot\mathbf{T}^m\right)\\
&\qquad + \mathbf{F}_T - \left(\frac{3}{2}\mathbf{K}_h^c(\mathbf{v}^n)\cdot\mathbf{H}^n - \frac{1}{2}\mathbf{K}_h^c(\mathbf{v}^{n-1})\cdot\mathbf{H}^{n-1}\right).
\end{aligned} \tag{11}$$

3. solve the above equations to obtain a new evaluation of temperature. Use it to update the enthalpy through Eq. (10)

4. repeat the process until a relative difference between two consecutive iterations of the total enthalpy is less than a given tolerance, i.e. $\max\left(\mathrm{abs}\left((H_i^{m+1} - H_i^m)/H_i^m\right)\right) < 10^{-4}$.

4. Mushy zone properties

Density of the mushy zone, due to the sixth assumption above, is equal to density of liquid and of solid, i.e. $\rho = \rho_L = \rho_S$. Both, the permeability and mixture thermal conductivity depend on the local structure of directional dendritic solidification, which leads to anisotropy of flow resistance and heat transfer in the two-phase region.

Permeability

Poirier [16] has shown that the permeability values in direction parallel and normal to the dendrites are significantly different from each other (even by orders in magnitude). Modeling the dendritic structure as a bank of cylinders and using the Blake–Kozeny model of flow in a porous medium, he has derived the following expressions for permeability along the dendrites and normal to them, respectively

$$K_{\parallel} = \frac{mf^3}{(1-f)^2}; \qquad K_{\perp} = \frac{mf^3}{(1-f)^{3/4}} \tag{12}$$

where m is the parameter which depends on the morphology of the two-phase region. It is determined through the analysis of the primary and secondary dendrite spacings [16]. Since the dendrites tend to grow in the direction along the local normal to the isotherm passing through the point [8, 19], this direction is taken as the primary one. In the model used in calculations the primary dendrite direction is specified at the moment when the *liquidus* isotherm passes through the point (see Fig. 1) and this direction is prevailed until the *solidus* isotherm crosses the point. Thus, the local structure

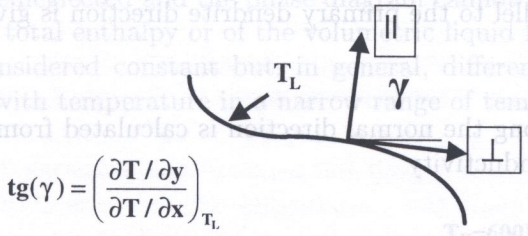

Fig. 1. Principal directions of dendrite growth and flow resistance

of the mushy zone is not varying in time but the solid fraction is increasing. This approach is slightly different that the one used in [19] where both the local structure and solid fraction are assumed to be varying. Thus, components of the inverse of the permeability tensor take the form

$$\begin{aligned} K_{xx}^{-1} &= \frac{1}{2}\left[\left(K_{\parallel}^{-1} + K_{\perp}^{-1}\right) + \left(K_{\parallel}^{-1} - K_{\perp}^{-1}\right)\cos(2\gamma)\right], \\ K_{xy}^{-1} &= K_{yx}^{-1} = \frac{1}{2}\left(K_{\perp}^{-1} - K_{\parallel}^{-1}\right)\sin(2\gamma), \\ K_{yy}^{-1} &= \frac{1}{2}\left[\left(K_{\parallel}^{-1} + K_{\perp}^{-1}\right) - \left(K_{\parallel}^{-1} - K_{\perp}^{-1}\right)\cos(2\gamma)\right], \end{aligned} \tag{13}$$

where (see Fig. 1)

$$tg(\gamma) = \left(\frac{\partial T/\partial y}{\partial T/\partial x}\right)_{T_L}. \tag{14}$$

Thermal conductivity

Thermal conductivity of the two-phase zone can be expressed as

$$\lambda_e = \lambda_e^0 + \lambda_e^d \tag{15}$$

where λ_e^0 and λ_e^d are the static and the dispersive terms, respectively.

Three different models of the static thermal conductivity in the mushy zone have been analyzed in the present study. The first one, further referred to as Model_1, is the commonly used mixture model

$$\lambda_e^0 = (1-f)\lambda_s + f\,\lambda_l\,. \tag{16}$$

It is a common practice to use the above expression in both the parallel and normal directions to get isotropic thermal conductivity model. From the theory of heterogeneous materials it is, however, known that the above model may be used only in special cases [1]. It is valid for layered configuration or bundles of unidirectional cylinders, when heat flow occurs solely along the layers or cylinders axis. In general, it is the upper Wiener bound of the mixture conductivity irrespective of its structure [9].

As the dendritic solidification leads to the directional structure, one should rather use the anisotropic model, referred to as Model_2 in further analysis, where components of the thermal conductivity tensor take the form

$$\begin{aligned}
\lambda_{xx}^0 &= \frac{1}{2}\left[(\lambda_{\parallel}+\lambda_{\perp}) + (\lambda_{\parallel}-\lambda_{\perp})\cos(2\gamma)\right],\\
\lambda_{xy}^0 &= \lambda_{yx}^0 = \frac{1}{2}(\lambda_{\parallel}-\lambda_{\perp})\sin(2\gamma),\\
\lambda_{yy}^0 &= \frac{1}{2}\left[(\lambda_{\parallel}+\lambda_{\perp}) - (\lambda_{\parallel}-\lambda_{\perp})\cos(2\gamma)\right],
\end{aligned} \tag{17}$$

where the conductivity parallel to the primary dendrite direction is given by

$$\lambda_{\parallel} = (1-f)\lambda_s + f\,\lambda_l\,, \tag{18}$$

whereas the conductivity along the normal direction is calculated from the lower Wiener bound of a heterogeneous material conductivity

$$\lambda_{\perp} = \frac{1-f}{\lambda_s} + \frac{f}{\lambda_l}\,. \tag{19}$$

To account for less regular structure, where dendrites can grow along different directions, the isotropic model of the averaged effective conductivity (Model_3) is proposed, where

$$\begin{aligned}
\lambda_{\parallel} &= (1-f)\lambda_s + f\,\lambda_l\,,\\
\lambda_{\perp} &= \frac{1-f}{\lambda_s} + \frac{f}{\lambda_l}\,,\\
\lambda_e^0 &= \sqrt{\lambda_{\parallel}\cdot\lambda_{\perp}}\,.
\end{aligned} \tag{20}$$

Thermal dispersion is also known to have a directional character [1]. Components λ_{ij}^d of the thermal dispersion tensor, for arbitrary direction of fluid flow, are given by

$$\begin{aligned}
\lambda_{xx}^d &= \lambda_{\perp}^d + \left(\lambda_{\parallel}^d - \lambda_{\perp}^d\right)\frac{v_x v_x}{|v|^2}\,,\\
\lambda_{xy}^d &= \lambda_{yx}^d = \left(\lambda_{\parallel}^d - \lambda_{\perp}^d\right)\frac{v_x v_y}{|v|^2}\,,\\
\lambda_{yy}^d &= \lambda_{\perp}^d + \left(\lambda_{\parallel}^d - \lambda_{\perp}^d\right)\frac{v_y v_y}{|v|^2}\,,
\end{aligned} \tag{21}$$

where $|v| = \sqrt{v_x^2 + v_y^2}$.

The principal axes of the tensor λ_{ij}^d are thus mainly determined by the direction of the fluid velocity vector $\mathbf{v}(v_x, v_y)$. When mixing of the fluid streams is the dominating mechanism of the thermal dispersion, then the principal values $\lambda_{||}^d$ and $\lambda_{\perp}^d$ of the dispersion tensor are proportional to

$$\lambda_{||}^d = (\rho_L c_L)\, c_{||} |\mathbf{v}| d, \qquad \lambda_{\perp}^d = (\rho_L c_L)\, c_{\perp} |\mathbf{v}| d, \tag{22}$$

where $c_{||}$ and $c_{\perp}$ are functions of the fluid volume fraction f and morphology of the porous medium, while d stands for mean dimension of pores (dendrite spacing). Following [13] and taking into account the expression for permeability along the dendrites and normal to them given by Eq. (12), these parameters can be calculated as

$$\begin{aligned} c_{\perp} &= 0.3718(1-f)^{2.4274}, \\ c_{||} &= 4c_{\perp}, \\ d &= \sqrt{80m}\,\frac{f}{1-f}. \end{aligned} \tag{23}$$

Total enthalpy

The mixture total enthalpy per cubic meter (ρH) is related to the phase enthalpies through

$$(\rho H) = (1-f)\rho_S H_S + f\rho_L H_L = \rho[(1-f)\, H_S + f H_L]. \tag{24}$$

However, in order to use the above expression the key relationship is needed between the liquid fraction, local temperature and concentration. In the analyzed simplified case of dilute systems where changes of concentration are neglected and the phase diagram cannot be used, some assumption on temperature changes of the total enthalpy or of the volumetric liquid fraction is needed. Therefore, phase specific heats are considered constant but, in general, different, and the total enthalpy is assumed linearly changing with temperature in a narrow range of temperature between the *solidus*

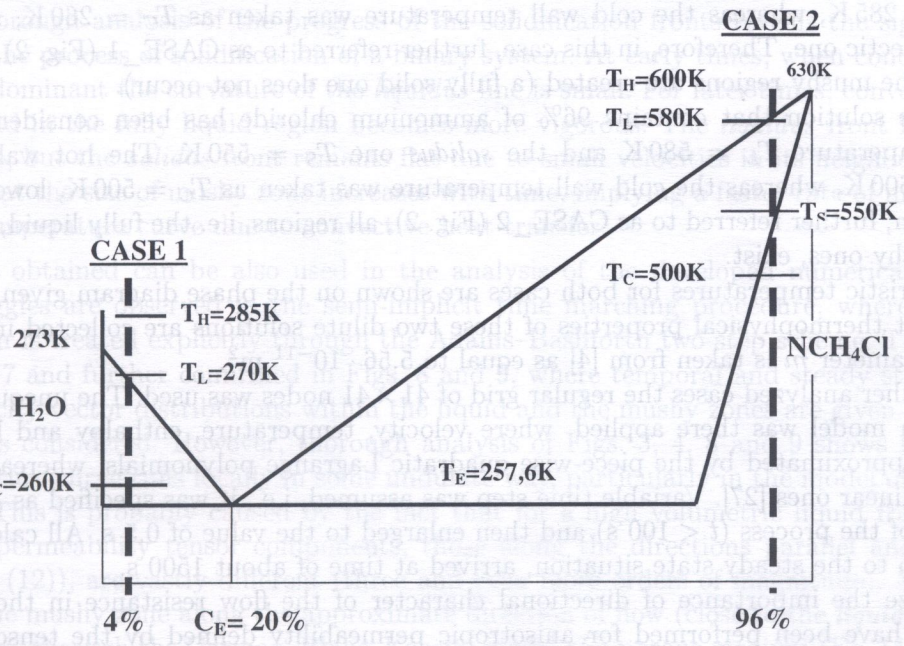

Fig. 2. Phase diagram for $NCH_4Cl + H_2O$ with specified characteristic temperatures of two dilute solutions analyzed

and the *liquidus* curves of a dilute solution (Fig. 2). The total enthalpy per cubic meter is given by Eq. (24), and specific enthalpy of the phases can be calculated as [19, 23]

$$\begin{aligned} H_S &= c_S T, \\ H_L &= c_S T + L(T), \end{aligned} \tag{25}$$

where the latent heat of solidification is the following function of temperature

$$L(T) = L(T_S) + (c_L - c_S)(T - T_S) \tag{26}$$

and by virtue of Eqs. (24), (25) and (26) the mixture specific enthalpy takes

$$H(T) = (1 - f)c_S T + f\left[c_S T + L(T_S) + (c_L - c_S)(T - T_S)\right]. \tag{27}$$

Using the assumed linear dependence of H on T, one can calculate from Eq. (27) the unknown volumetric liquid fraction f at a current local temperature T.

5. Results and discussion

The above mushy zone properties have been incorporated into the developed FEM computer simulation model and the code has been exploited to address the question of how the anisotropic morphology of the dendritic region influences the flow pattern and temperature field in this two-phase zone.

As an example the solidification of two different dilute solutions of ammonium chloride and water in a square cavity, of a side length equal to 0.025 m, has been calculated. Lower and upper horizontal walls of the cavity were assumed adiabatic, whereas the lateral walls were kept at constant but different temperatures. The right hot wall had temperature T_H equal to the initial one T_i. The sudden drop of the left wall temperature from T_i to T_C caused cooling and solidification of the solution confined in the cavity.

First, the binary system of 4% of ammonium chloride (much less than the eutectic concentration $C_E = 20\%$) has been analyzed, where the *liquidus* temperature $T_L = 270\,\mathrm{K}$ and the *solidus* temperature was equal to the eutectic one, i.e. $T_S = T_E = 257.6\,\mathrm{K}$. The hot wall was kept at $T_H = T_i = 285\,\mathrm{K}$, whereas the cold wall temperature was taken as $T_C = 260\,\mathrm{K}$, slightly higher than the eutectic one. Therefore, in this case, further referred to as CASE_1 (Fig. 2), only the fully liquid and the mushy regions are created (a fully solid one does not occur).

Next, the solution that contains 96% of ammonium chloride has been considered, where the *liquidus* temperature $T_L = 580\,\mathrm{K}$ and the *solidus* one $T_S = 550\,\mathrm{K}$. The hot wall was kept at $T_H = T_i = 600\,\mathrm{K}$, whereas the cold wall temperature was taken as $T_C = 500\,\mathrm{K}$, lower than T_S. In this situation, further referred to as CASE_2 (Fig. 2), all regions, i.e. the fully liquid, the fully solid and the mushy ones, exist.

Characteristic temperatures for both cases are shown on the phase diagram given in Fig. 2, and the pertinent thermophysical properties of these two dilute solutions are collected in Table 1. [12, 26]. The parameter m is taken from [4] as equal to $5.56 \cdot 10^{-11}\ \mathrm{m}^2$.

In all further analyzed cases the regular grid of 41×41 nodes was used. The unequal order FEM interpolation model was there applied, where velocity, temperature, enthalpy and liquid fraction fields were approximated by the piece-wise quadratic Lagrange polynomials, whereas the pressure field by the linear ones [27]. Variable time step was assumed, i.e., it was specified as $\Delta t = 0.25$ s at early times of the process ($t < 100$ s) and then enlarged to the value of 0.5 s. All calculations were continued up to the steady state situation, arrived at time of about 1500 s.

To analyze the importance of directional character of the flow resistance in the mushy zone, calculations have been performed for anisotropic permeability defined by the tensor K_{ij}. Equations (13) and (14) give components of the permeability tensor inverse. The results thus obtained have been compared to those received from the isotropic model, where permeability of the mushy

Table 1. Physical properties of two dilute solutions analyzed

CASE_1	CASE_2
$\rho_L = \rho_S = 1016\,\mathrm{kg/m^3}$	$\rho_L = \rho_S = 1078\,\mathrm{kg/m^3}$
$c_{pL} = 4.187\,\mathrm{kJ/(kgK)}$	$c_{pL} = 3.249\,\mathrm{kJ/(kgK)}$
$c_{pS} = 1.567\,\mathrm{kJ/(kgK)}$	$c_{pS} = 1.870\,\mathrm{kJ/(kgK)}$
$\lambda_L = 0.582\,\mathrm{W/(mK)}$	$\lambda_L = 0.486\,\mathrm{W/(mK)}$
$\lambda_S = 2.500\,\mathrm{W/(mK)}$	$\lambda_S = 0.393\,\mathrm{W/(mK)}$
$L = 318\,\mathrm{kJ/kg}$	$L = 307\,\mathrm{kJ/kg}$

zone is independent of direction and specified by $K_{xx} = K_{yy} = K_{||}$ with $K_{xy} = K_{yx} = 0$. In all these calculations the isotropic model of averaged effective conductivity (Model_3) was used and thermal dispersion was neglected.

Temporal flow pattern, the mushy zone shape (confined by the *solidus* and the *liquidus* isotherms) and lines of constant volumetric liquid fraction in this region are compared in Figs. 3 and 4, respectively, for CASE_1 and CASE_2 of the analyzed dilute solutions. In addition, Fig. 5 shows the evolution of the mushy zone predicted by both the isotropic and anisotropic permeability models. From these comparisons, one can conclude that anisotropy of the mushy zone permeability visibly alters the shape of the liquidus phase front making it less distorted (both CASE_1 and CASE_2 in Figs. 3, 4 and 5). The form of the solidus boundary of the two-phase region, is, however, much less influenced (CASE_2 in Figs. 4 and 5). Figures 6 and 7 show steady state distributions of the volumetric liquid fraction and the local velocity vector length in the mushy zone in three different horizontal cross sections of the cavity, situated at one-fourth, one-half and three-fourth of the cavity height. The velocity in the two-phase region is much smaller in magnitude for the anisotropic case. This results from the fact that the permeability along isotherms, i.e., in the approximate direction of flow in the mushy zone, is much less than in the isotropic model of flow resistance. Therefore, the smaller curvature of shapes of the phase fronts is observed for the anisotropic situation (Figs. 3–5).

Further, thorough analysis of the progress of the solidification fronts reveals the significance of convection in the process of solidification of a binary system. At early times, when conduction heat transfer is predominant the curvature of the *liquidus* line is small. For later times, convection in the mushy zone and in the fully liquid region becomes more vigorous. The *liquidus* front line assumes a curved shape; but the *solidus* front remains flat due to small velocities in its neighborhood. It is also evident that the size of mushy zone increases with time, implying a faster rate of movement for the *liquidus* temperature curve due to convective heat transfer.

The results obtained can be also used in the analysis of the developed numerical simulation model. No wiggles are observed in the semi-implicit time marching procedure, where the advection/convection is treated explicitly through the Adams–Bashforth two-step scheme. This is visible in Figs. 6 and 7 and further confirmed in Figs. 8 and 9, where temporal and steady state (at time = 1500 s) velocity vector distributions within the liquid and the mushy zones are given for the both dilute solutions considered. However, thorough analysis of Figs. 3, 4, 8 and 9 shows that the *liquidus* temperature curve runs locally in some undulate way, particularly in the model of anisotropic permeability. This is probably caused by the fact that for a high volumetric liquid fraction (close to unity) the permeability tensor components, those along the directions parallel and normal to dendrites (Eq. (12)), are vastly different (three and even more orders of magnitude). Much higher resistance of the mushy zone along the approximate direction of flow (close to the *liquidus* temperature line) causes, through the Carman–Blake–Kozeny model of a porous medium (Eq. (4)), a sudden vanishing of velocity at some adjacent points. These local irregularities in the velocity distribution are not observed in the case of isotropic permeability model (Figs. 8 and 9).

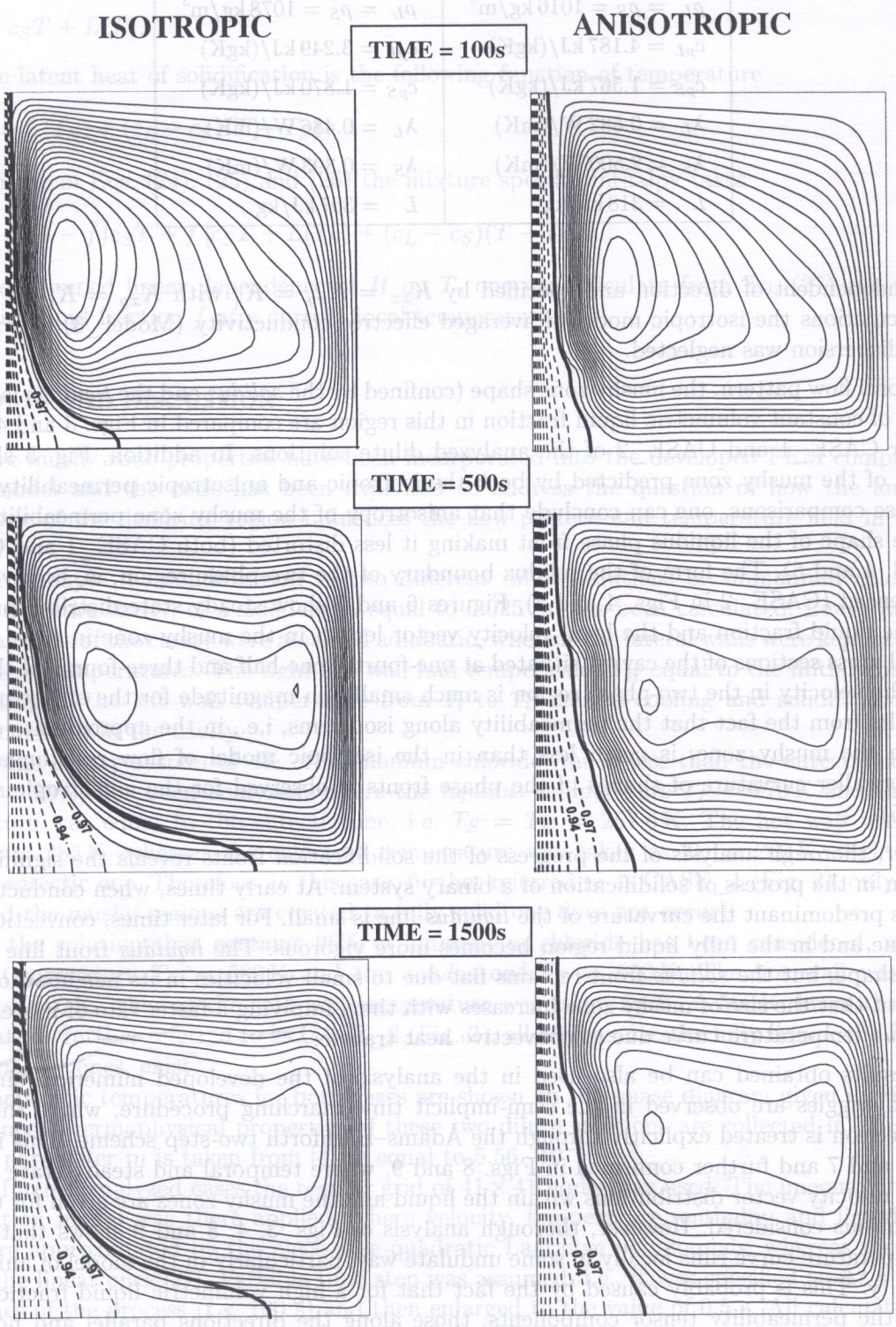

Fig. 3. Streamlines and lines of constant liquid fraction for CASE_1 of dilute solution

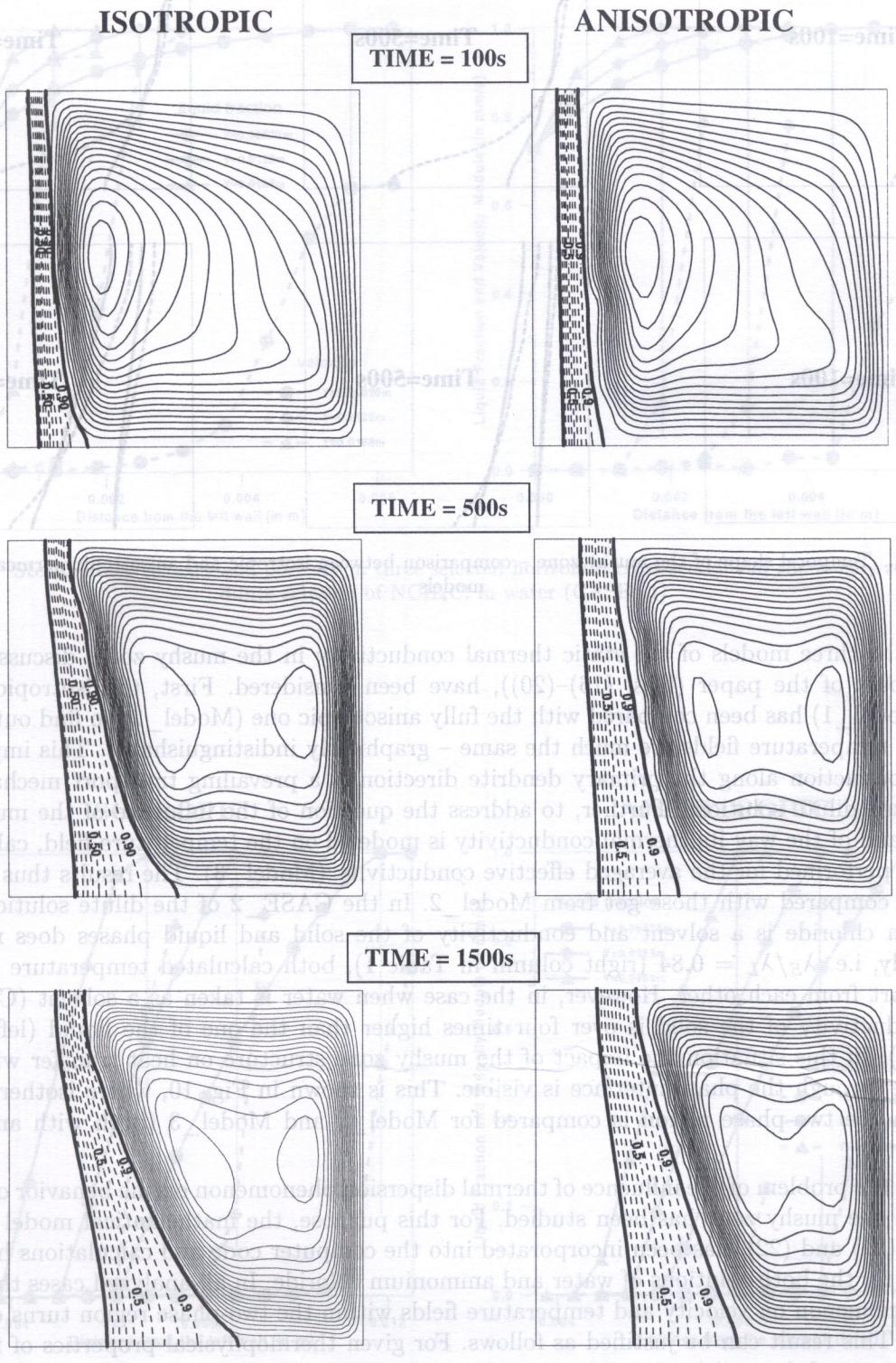

Fig. 4. Streamlines and lines of constant liquid fraction for CASE_2 of dilute solution

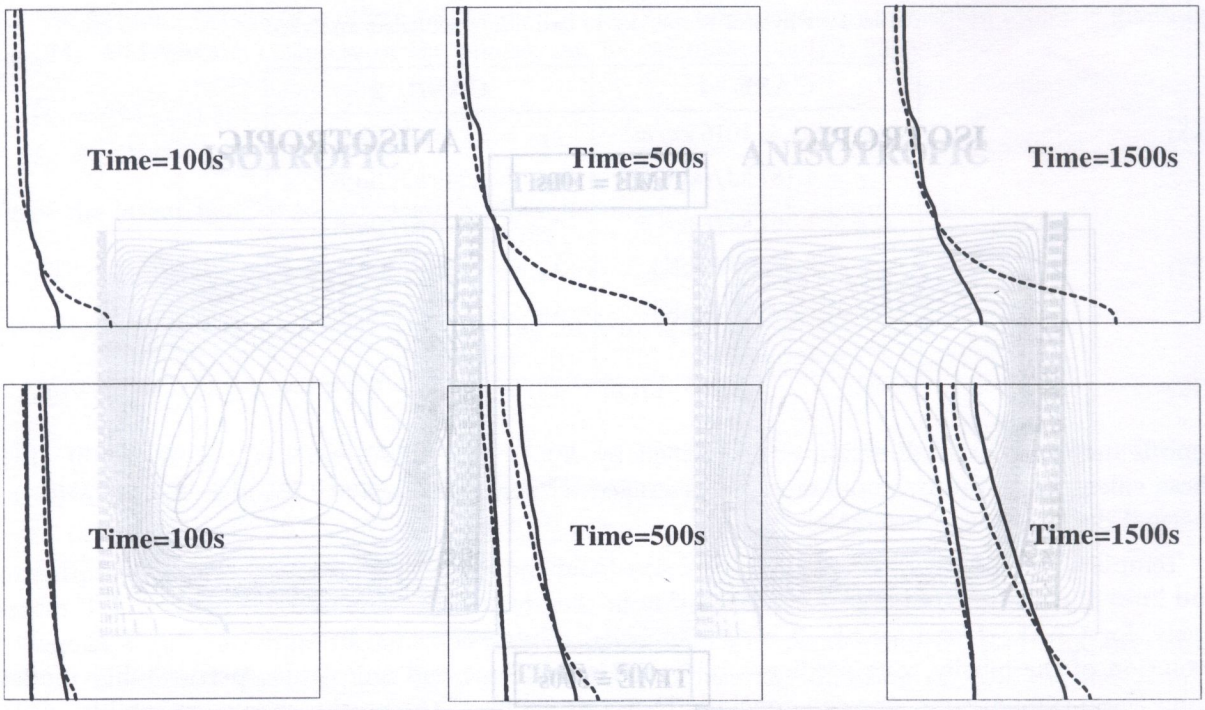

Fig. 5. Temporal shape of the mushy zone – comparison between isotropic and anisotropic permeability models

Next, the three models of the static thermal conductivity in the mushy zone, discussed in the previous part of the paper (Eqs. (16)–(20)), have been considered. First, the isotropic mixture model (Model_1) has been compared with the fully anisotropic one (Model_2) to find out that the calculated temperature fields are much the same – graphically indistinguishable. This implies that thermal conduction along the primary dendrite direction is a prevailing transport mechanism for the analyzed dilute solutions. Further, to address the question of the influence of the mushy zone structure and of the way its thermal conductivity is modeled on the temperature field, calculations have been performed for the averaged effective conductivity (Model_3). The results thus obtained have been compared with those got from Model_2. In the CASE_2 of the dilute solution, where ammonium chloride is a solvent and conductivity of the solid and liquid phases does not differ significantly, i.e. $\lambda_S/\lambda_L = 0.84$ (right column in Table 1), both calculated temperature fields are hardly apart from each other. However, in the case when water is taken as a solvent (CASE_1), phase conductivity of the solid is over four times higher than the one of the liquid (left column of Table 1). In this situation the impact of the mushy zone structure on heat transfer within this region and through the phase interface is visible. This is shown in Fig. 10, where isothermal lines run within the two-phase region is compared for Model_2 and Model_3 (both with anisotropic permeability).

Finally, the problem of the influence of thermal dispersion phenomenon on the behavior of a dilute solution in the mushy zone has been studied. For this purpose, the mathematical model given by Eqs. (15), (21) and (22), has been incorporated into the computer code and calculations have been performed for the both solutions of water and ammonium chloride. In all analyzed cases the impact of this phenomenon on velocity and temperature fields within the two-phase region turns out to be negligible. This result can be justified as follows. For given thermophysical properties of fluid, the dispersive term of thermal conductivity depends on both the porosity f and the local velocity $|\mathbf{v}|$ (Eqs. (22) and (23)). This dependence is given by $\lambda^d \sim F(f)|\mathbf{v}|$, where $F(f) = f/(1-f)^{1.4274}$. Function $F(f)$ takes its maximal value at $f = 0.412$. On the other hand, for analyzed NCH_4Cl+H_2O solutions, where the parameter m is very small, the velocity swiftly diminishes in the mushy zone (Figs. 6 and 7). It's magnitude is of the order of 10^{-3} m/s in the region adjacent to the *liquidus*

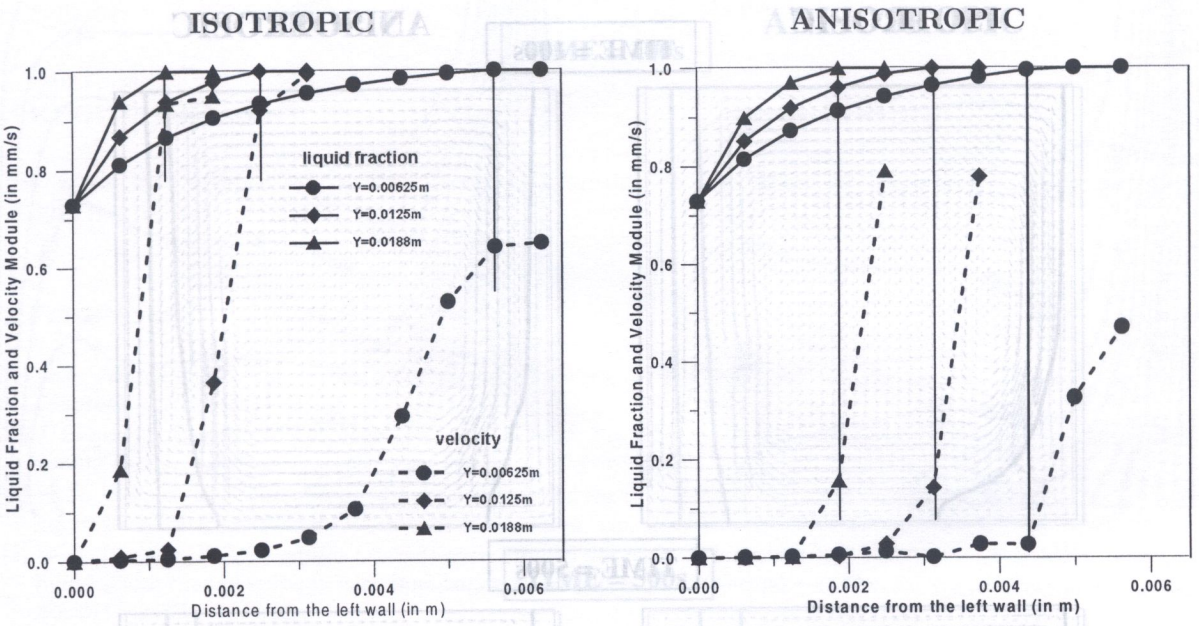

Fig. 6. Steady-state velocity and porosity in three selected horizontal cross-sections of the mushy zone for dilute solution of NCH_4Cl in water (CASE_1)

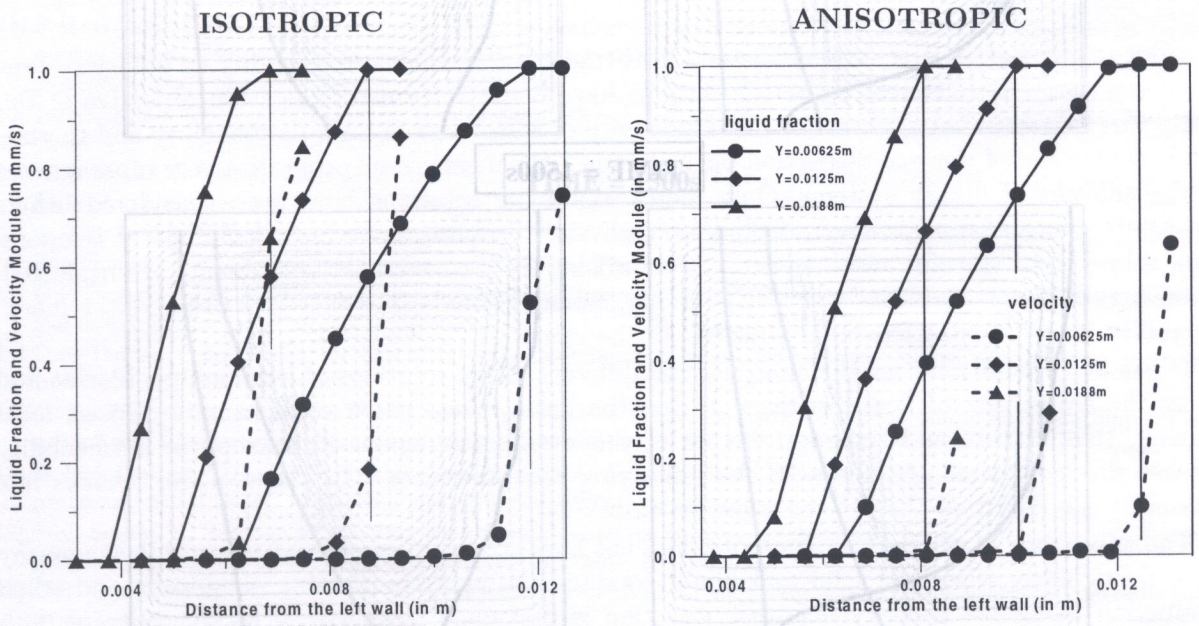

Fig. 7. Steady-state velocity and porosity in three selected horizontal cross-sections of the mushy zone for dilute solution of H_2O in ammonium chloride (CASE_2)

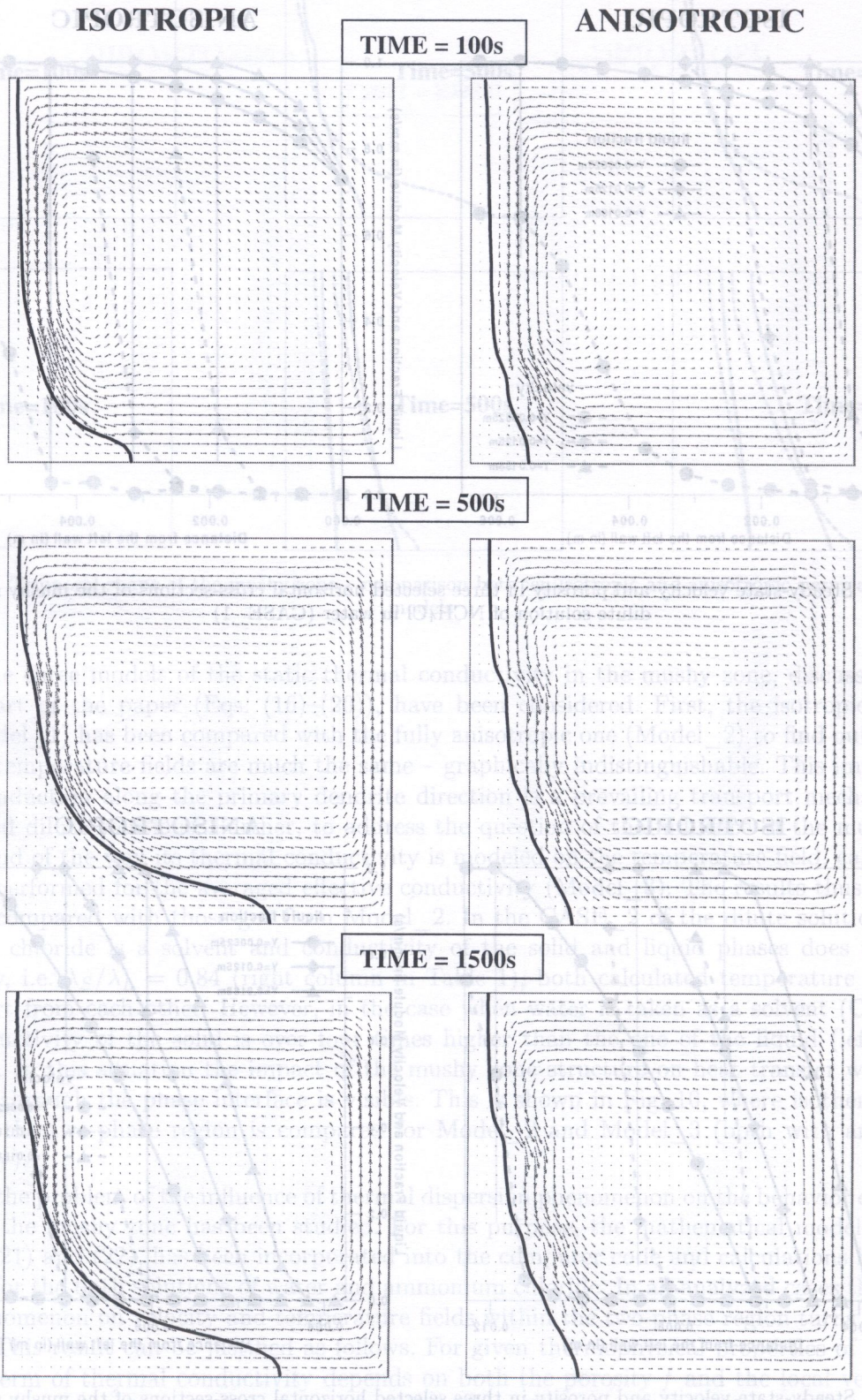

Fig. 8. Temporal velocity field and the *liquidus* temperature line for CASE_1 of dilute solution

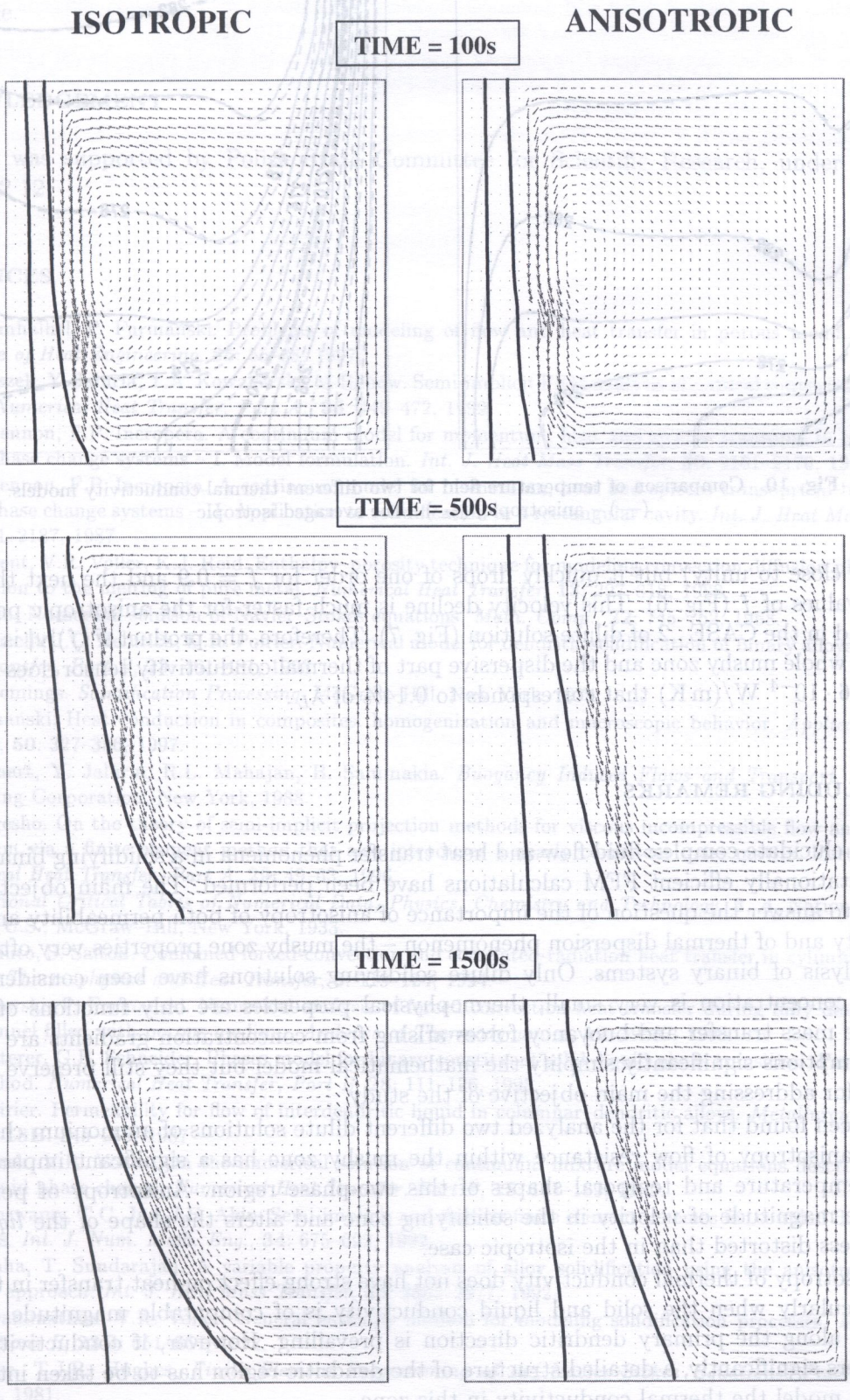

Fig. 9. Temporal velocity field and the *liquidus* temperature line for CASE_2 of dilute solution

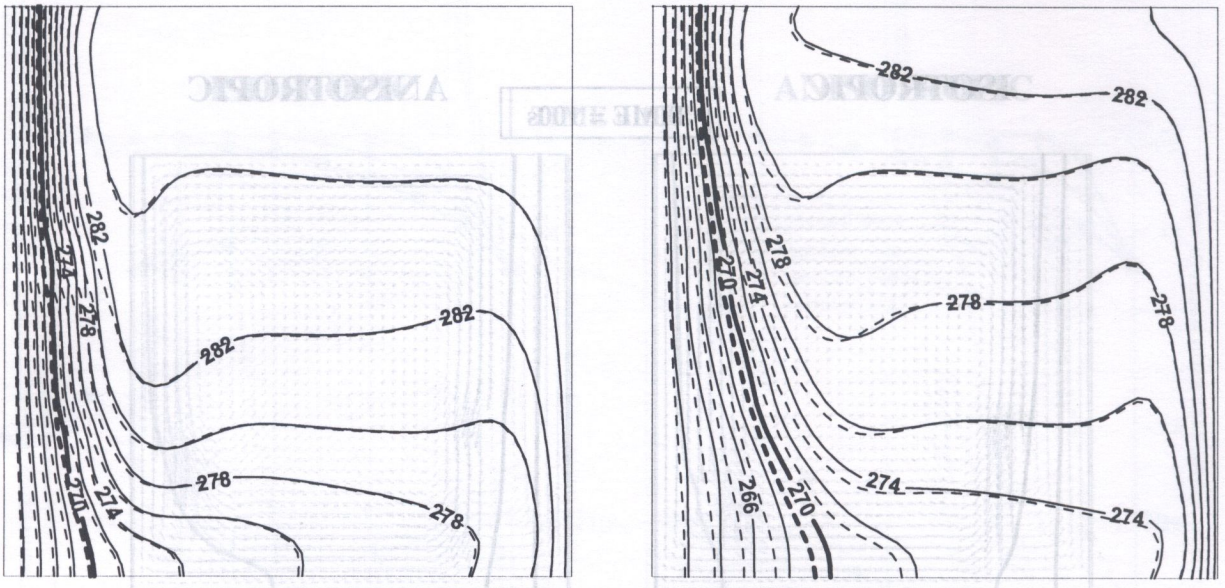

Fig. 10. Comparison of temperature field for two different thermal conductivity models: (—) – anisotropic, (---) – the averaged isotropic

line (for f close to unity) but it quickly drops of one order for $f = 0.9$ and the next three orders for lower values of f (Fig. 6). This velocity decline is much faster for the anisotropic permeability (Fig. 6) and in the CASE_2 of dilute solution (Fig. 7). Therefore, the product $F(f)|\mathbf{v}|$ is very small within the whole mushy zone and the dispersive part of thermal conductivity tensor does not exceed a value of $6 \cdot 10^{-4}$ W/(m K) that corresponds to 0.14% of λ_L .

6. Concluding remarks

In order to elucidate complex fluid flow and heat transfer phenomena in a solidifying binary system, the computationally efficient FEM calculations have been performed. The main objective of this study was to answer the question of the importance of anisotropy of both permeability and thermal conductivity and of thermal dispersion phenomenon – the mushy zone properties very often ignored in the analysis of binary systems. Only dilute solidifying solutions have been considered, where the solute concentration is very small, thermophysical properties are only functions of temperature, solute mass transfer and buoyancy forces arising from concentration gradients are neglected. These assumptions significantly simplify the mathematical model but they still preserve the model capability for addressing the main objective of the study.

It has been found that for the analyzed two different dilute solutions of ammonium chloride and water the anisotropy of flow resistance within the mushy zone has a significant impact on local velocity, temperature and temporal shapes of this two-phase region. Anisotropy of permeability reduces the magnitude of velocity in the solidifying zone and alters the shape of the *liquidus* line making it less distorted than in the isotropic case.

The anisotropy of thermal conductivity does not have strong effect on heat transfer in the mushy zone, particularly when the solid and liquid conductivity is of comparable magnitude and when conduction along the primary dendritic direction is prevailing. However, if conductivity of both phases differs significantly, a detailed structure of the dendritic region has to be taken into account to properly model the thermal conductivity in this zone.

Thermal dispersion is the phenomenon that always occurs in the dendritic region because it is caused by the mixing of the local fluid streams passing through tortuous paths around solid dendrites and by the enhancement of the mutual solid–fluid thermal interaction. However, in the

analyzed case of the ammonium chloride and water solutions, where the permeability and velocity are small, the impact of this phenomenon on the behavior of the binary system in the mushy zone is negligible.

ACKNOWLEDGEMENT

This work was supported by Polish State Committee for Scientific Research, under grant No. 3 T09C 002 12.

REFERENCES

[1] G.A. Amhalhel, P. Furmański. Problems of modeling of flow and heat transfer in porous media. *Bulletin of Institute of Heat Engineering*, **85**: 55–88, 1997.

[2] J. Banaszek, Y. Jaluria, T.A. Kowalewski, M.Rebow. Semi-implicit FEM analysis of natural convection in freezing water. *Numerical Heat Transfer, Part A.*, **36**: 449–472, 1999.

[3] W.D. Bennon, F.P. Incropera. A continuum model for momentum, heat and spieces transoprt in binary solid–liquid phase change systems – I. Model formulation. *Int. J. Heat Mass Transfer*, **30**: 2161–2170, 1987.

[4] W.D. Bennon, F.P. Incropera. A continuum model for momentum, heat and spieces transoprt in binary solid–liquid phase change systems – II. Application to solidification in a rectangular cavity. *Int. J. Heat Mass Transfer*, **30**: 2171–2187, 1987.

[5] A.D. Brent, V.R. Voller, K.J. Reid. Enthalpy–porosity technique for modeling convection diffusion phase change: application to the melting of pure metal. *Numerical Heat Transfer*, **13**: 297–318, 1988.

[6] J. Chorin. Numerical solution of Navier–Stokes equations. *Math. Comp.*, **22**: 745–762, 1968.

[7] S.D. Felicelli, J.C. Heinrich, D.R. Poirier. Numerical model for dendritic solidification of binary alloys. *Numerical Heat Transfer, Part B*, **23**: 461–481, 1993.

[8] M.C. Flemings. *Solidification Processing.* McGraw–Hill, New York, 1974.

[9] P. Furmański. Heat conduction in composites: homogenization and macroscopic behavior. *Applied Mechanics Reviews*, **50**: 327–356, 1997.

[10] B. Gebhart, Y. Jaluria, R.L. Mahajan, B. Sammakia. *Buoyancy Induced Flows and Transport.* Hemisphere Publishing Corporation, New York, 1988.

[11] P.M. Gresho. On the theory of semi-implicit projection methods for viscous incompressible flow and its implementation via a finite element method that also introduces a nearly consistent mass matrix. Part 1: Theory. *Numerical Heat Transfer, Part A*, **29**: 49–63, 1996.

[12] *International Critical Tables of Numerical Data, Physics, Chemistry and Technology.* **3, 4**. National Research Council U.S., McGraw–Hill, New York, 1933.

[13] K. Kamiuto, S. Saitoh. Combined forced-convection and correlated-radiation heat transfer in cylindrical patches beds. *J. Thermophysics and Heat Transfer*, **8**: 119–124, 1994.

[14] A. Mitrowski, P. Furmański. Numerical analysis of forced convection heat transfer during fully developed flow in a channel filled with porous medium. *Archives of Thermodynamics*, **19**: 39–57, 1998.

[15] G.F. Naterer, G.E. Schneider. Phases model for binary-constituent solid–liquid phase transition. Part 1: Numerical method. *Numerical Heat Transfer, Part B*, **28**: 111–126, 1995.

[16] D.R. Poirier. Permeability for flow of interdendritic liquid in columnar–dendritic alloys. *Metallurgical Transactions B*, **18B**: 245–255, 1987

[17] C. Prakash, V.R. Voller. On the numerical solution of continuum mixture model equations describing binary solid–liquid phase change. *Numerical Heat Transfer, Part B*, **15**: 171–189, 1989.

[18] B. Ramaswamy, T.C. Jue, J.E. Akin. Semi-implicit and explicit finite element schemes for coupled fluid/thermal problems. *Int. J. Num. Meth. Eng.*, **34**: 675–692, 1992.

[19] S.K. Sinha, T. Sundarajan. A variable property analysis of alloy solidification using the anisotropic porous medium approach. *Int. J. Heat Mass Transfer*, **35**: 2865–2877, 1992.

[20] C.R. Swaminathan, V.R. Voller. General enthalpy method for modeling solidification processes. *Metallurgical Transactions B*, **23B**: 651–664, 1992.

[21] C. Taylor, T.J.R. Hughes. *Finite Element Programming of the Navier–Stokes Equations.* Pineridge Press, Swansea, 1981.

[22] S. Usmani, R.W. Lewis, K.N. Seetharamu. Finite element modelling of natural convection-controlled change phase. *Int. J. Num. Meth. in Fluids*, **14**: 1019–1036, 1992.

[23] V.R. Voller, A.D. Brent, C. Prakash. The modeling of heat, mass and solute transport in solidification systems. *Int. J. Heat Mass Transfer*, **32**: 1719–1731, 1989.

[24] V.R. Voller, M. Cross, N.C. Markatos. An enthalpy method for convection/diffusion phase change. *Int. J. Num. Meth. Eng.*, **24**: 271–284, 1987.

[25] V.R. Voller, C. Prakash. A fixed grid numerical modeling methodology for convection–diffusion mushy region phase-change problems. *Int. J. Heat and Mass Transfer*, **30**: 1709–1719, 1987.

[26] X. Zeng, A. Faghri. Temperature transforming model for binary solid–liquid phase-change problems. Part I: Mathematical modeling and numerical methodology, Part II: Numerical simulation. *Numerical Heat Transfer, Part B*, **25**: 467–480 and 481–500, 1993.

[27] O.C. Zienkiewicz and R.L. Taylor. *Finite element method.* Fourth Edition, McGraw–Hill, London, 1989.